Ultrastructural Localization of Albumin Transport across the Cerebral Microvasculature during Experimental Meningitis in the Rat

By Vincent J. Quagliarello,* Anne Ma,* Hans Stukenbrok,‡ and George E. Palade‡

*From the Departments of *Internal Medicine and ‡Cell Biology, Yale University School of Medicine, New Haven, Connecticut 06510*

Summary

Injury to the blood brain barrier (BBB) is a fundamental sequela of bacterial meningitis, yet the precise mechanism facilitating exudation of albumin across the endothelium of the cerebral microvasculature remains conjectural. After intracisternal inoculation of *Escherichia coli* (0111:B4) lipopolysaccharide in rats to elicit a reversible meningitis and BBB injury, we utilized in situ tracer perfusion and immunolabeling procedures to identify by transmission electron microscopy the precise topography and microvascular exit pathway(s) of bovine serum albumin (BSA). Results revealed that during meningitis there was: (*a*) an inducible increase in immunodetectable monomeric BSA binding to the luminal membrane of all microvascular segments in the pia-arachnoid and superficial brain cortex; (*b*) similar uptake of both colloidal Au-BSA (as well as monomeric BSA) by plasmalemmal vesicles but no detectable transcytosis to the abluminal side; and (*c*) predominant exit of both perfused Au-BSA and immunodetectable monomeric BSA through open intercellular junctions of venules in the pia-arachnoid. This was corroborated in separate experiments documenting focal pial venular leaks of in situ perfused 0.01% colloidal carbon black during experimental meningitis. These results provide precise localization of BBB injury in meningitis to meningeal venules, confirm a paracellular exit pathway of albumin via open intercellular junctions, and suggest an injury mechanism amenable to specific therapeutic intervention.

Bacterial meningitis remains a common disease with unacceptable morbidity and mortality despite bactericidal antibiotic therapy. This observation supports the hypothesis that pathophysiologic sequelae of the disease progress despite bacteriologic cure and effect irreversible neuronal injury (1). The blood brain barrier (BBB)[1] represents one critical site functionally injured in meningitis, with the resultant central nervous system protein exudation a physiologic precipitant of vasogenic brain edema. Anatomically, investigation has localized the cerebral microvasculature as the major site responsible for the BBB due to its unique ultrastructural features: primarily rare plasmalemmal vesicles and continuous intercellular tight junctions (2–4). These unique features impart upon it the characteristics of a high resistance endothelium (5), allowing it to function as a barrier to macromolecular (i.e., albumin) transport as well as to facilitate integration of neuronal synaptic information.

In systemic microvasculature, ultrastructural mechanisms of albumin transport have been recently investigated. Specifically, using the method of in situ administration of colloidal gold-albumin complexes, evidence exists that there are specific luminal membrane binding microdomains for albumin. Topographically, they appear restricted to uncoated pits and plasmalemmal vesicles that appear to function in receptor-mediated transcytosis (6). Therefore, a major question arises from a clinical and biological perspective as to the precise mechanism facilitating albumin exudation across the cerebral microvasculature during infectious injury. In this inquiry, using a rat model of meningitis, we sought to investigate three basic questions. (*a*) What is the topographic location of cerebral microvascular injury during meningeal inflammation? Is it localized to the leptomeninges, or does it extend to the parenchymal microvasculature? (*b*) Which microvascular segments (i.e., arteriolar, capillary, or venular) are predominantly affected? (*c*) Is there evidence of a primary transcellular or paracellular pathway of albumin exit out of the microvasculature during meningitis? To investigate these questions, we utilized in situ perfusion of colloidal gold-BSA complexes as well as immunogold labeling of perfused monomeric

[1] *Abbreviations used in this paper:* BBB, blood brain barrier; PV, plasmalemmal vesicles; RSA, endogenous rat serum albumin; TEM, transmission electron microscopy.

J. Exp. Med. © The Rockefeller University Press • 0022-1007/91/09/0657/16 $2.00
Volume 174 September 1991 657–672

BSA to localize, by transmission electron microscopy (TEM), albumin exit pathways during experimental meningitis.

Materials and Methods

Materials

$HAuCl_4$, BSA, OVA, poly-L-glutamic acid (mol wt, 15,000–50,000), and biotinylated goat anti-rat IgG were purchased from Sigma Chemical Co. (St. Louis, MO). *Escherichia coli* 0111:B4 LPS was a gift from Dr. J. Ryan, Yale University. 125-I BSA was purchased from ICN Radiochemicals (Irvine, CA). M 199 powder was obtained from Gibco Laboratories, (Grand Island, NY), and Freund's adjuvant from Difco Laboratories (Detroit, MI). Protein G was bought from Pierce Chemical Co. (Rockford, IL). Goat anti-rat IgG-Au(5nm) was obtained from Janssen Life Sciences Products (Piscataway, NJ). Ketamine was bought from Parke Davis (Morris Plains, NJ), and Xylazine from Miles Laboratories (Shawnee, KS). Butterfly needles were purchased from Abbott (North Chicago, IL), and glutaraldehyde, propylene oxide, Epon, and uranyl acetate were obtained from E.M. Sciences (Ft. Washington, PA).

Preparation of Colloidal Gold-BSA Tracer

Colloidal gold particles with mean diameter of 5 nm were prepared by reducing $HAuCl_4$ with a combination of Na citrate and tannic acid as previously described (7). After a 72-h dialysis vs. ddH_2O, the optimal ligand (BSA) coupling concentration was determined to be 80 μg/ml by the NaCl aggregation method. BSA (80 μg/ml of a previously dialyzed 1% BSA solution) was then coupled to the colloidal gold solution, stabilized with poly-L-glutamic acid (200 μg/ml of a previously dialyzed 1% solution), and ultracentrifuged (180,000 *g* for 45 min) with the soft pellet resuspended in PBS-glutamic acid (200 μg/ml), and the OD_{520} adjusted to 1.0 for perfusion experiments. As a control tracer solution, colloidal gold uncoupled to protein was stabilized with the poly-L-glutamic acid, ultracentrifuged, and diluted to OD_{520} = 1.0 analogous to the method for colloidal gold-BSA. Tracer solutions were kept at 4°C, documented to be monodisperse by TEM before use, and were utilized for perfusions within 2 h of preparation.

Induction of Experimental Meningitis

The technique used was previously described (8). Adult male Wistar rats (125 gm) were anesthetized with ketamine (100 mg/kg)/xylazine (7 mg/kg) by the intramuscular route. After removal of 75 μl of CSF by intracisternal puncture using a 25-gauge butterfly needle, 50 μl of LPS solution (containing 25 ng of *E. coli* 0111:B4 purified LPS) was injected intracisternally into each experimental animal with 50 μl of pyrogen-free saline inoculated into controls. After defined durations of disease development, meningitis was confirmed histologically by light microscopy, and CSF pleocytosis was quantitated by a second cisternal puncture using standard hemocytometry to determine the natural history of the CSF inflammatory response in vivo. Similarly, the onset, peak, and duration of functional BBB injury was determined by CSF penetration of systemically administered ^{125}I-BSA (10 μCi) 1 h before the second cisternal puncture. At the time of this second cisternal puncture, CSF and blood samples were simultaneously obtained for radioactive assay in a Gamma 300 counter (Beckman Instruments Inc., Irvine, CA). As previously described, only CSF samples without visible blood contamination were evaluated and the percent CSF penetration of ^{125}I-BSA was determined from the equation: 100 × ^{125}I cpm per ml CSF/^{125}I cpm per ml blood.

In Situ Perfusion Protocols during Experimental Meningitis

Colloidal Gold-BSA Experiments. At the time of peak CSF inflammation and functional CSF transport of ^{125}I-BSA (4 h post-LPS intracisternal inoculation), rats were anesthetized, a thoracotomy was done, and the vasculature was perfused in situ in four sequential steps via the left ventricle with the right atrium cut to allow perfusate outflow: (*a*) a flush with oxygenated M199 media supplemented with glucose and HCO_3 ("supplemented M199") at 37°C, pH 7.4, using a perfusion rate of 15 ml/min for 10 min to ensure optimal CNS perfusion; (*b*) perfusion with Au-BSA (stabilized with poly-L-glutamic acid) solution (OD_{520} = 1.0) at the 15-ml/min flow rate for 10 min; (*c*) repeat flush with supplemented M199 media at 15 ml/min for 1 min; (*d*) in situ fixation with 3% glutaraldehyde in 0.1 M Na cacodylate, pH 7.4, supplemented with 0.1 mM $MgCl_2$ and 0.1 mM $CaCl_2$ at 15 ml/min for 10 min. Control groups included rats inoculated intracisternally with PBS (i.e., uninflamed controls), as well as rats inoculated with LPS (inflamed rats) in which the perfusion step consisted of colloidal gold stabilized by glutamic acid alone. After in situ fixation, cerebral cortex with intact pia was removed, cut into 5-mm cubes, placed in 2% osmium tetroxide, stained en bloc with 2% uranyl acetate, followed by standard embedding in Epon 812. Thin sections cut on an ultramicrotome were then stained with uranyl acetate and lead citrate and examined with TEM.

Carbon Black Perfusion Experiments. To assess the topography of the leptomeningeal injury, animals inoculated intracisternally with LPS (and controls) were perfusion fixed in situ in one step via the left ventricle with a 0.01% carbon black (vol/vol) solution in 3% glutaraldehyde (supplemented with 0.1 mM $MgCl_2$ and 0.1 mM $CaCl_2$ as before) at 15 ml/min for 10 min. The pial surface was then examined at 40× using a dissecting microscope and photographed to detect areas of carbon leak.

Immunolocalization of BSA after Experimental Meningitis

Production of Primary Antibody. 125-gm rats were immunized with various concentration of BSA (50–250 μg) in Freund's adjuvant. After the fourth injection, serum was collected, and rat anti-BSA Ig G was purified by protein G affinity chromatography with confirmation by SDS-PAGE. Purified antibody was kept frozen (−70°C) in 10-μl aliquots before use.

ELISA Determination of Optimal Fixation Conditions. To determine the optimal concentration of aldehyde fixation for in situ BSA immunolocalization, ELISAs were performed using BSA as antigen and the purified rat anti-BSA Ig G as primary antibody in the face of different fixative concentrations. From this, the sensitivity and specificity of the primary antibody were tested in the setting of different aldehyde fixative concentrations to determine optimal conditions for BSA immunodetection in situ.

In Situ Perfusion with Monomeric Tracer Free BSA. At a similar time of peak CSF inflammation (4 h post-LPS inoculation), anesthesia and thoracotomy were performed, and the vasculature similarly perfused in situ in sequential steps: (*a*) a flush with oxygenated supplemented M199 at 37°C using a 15-ml/min flow rate for 10 min; (*b*) perfusion with 40 mg/ml of a monomeric BSA (fraction V) solution for different time intervals (1 min, 10 min) at the same 15-ml/min flow rate; (*c*) in situ fixation with 4% paraformaldehyde/0.5% glutaraldehyde in 0.1 M Na cacodylate (pH 7.4).

Immunofluorescent BSA Localization In Situ. To determine the ability of the primary anti-BSA antibody to localize BSA perfused in situ, heart and brain cortices were cut into 1-mm coronal slices, frozen in liquid N_2, and cryosectioned (5-μm thickness) on a Frigocut (Reichert Scientific Instruments, Buffalo, NY). Cryostat

sections were then treated in the following way: (*a*) incubated with rat-anti-BSA (1:200 dilution in PBS, 1% OVA) for 1 h at room temperature; (*b*) washed with PBS, 1% OVA (PBSO) for 1 h; (*c*) incubated with biotinylated goat anti-rat IgG (1:500 in PBSO); (*d*) washed with PBSO for 1 h; (*e*) incubated with streptavidin-Texas Red (1:500 in PBSO); (*f*) washed with PBSO for 1 h and observed under phase contrast and fluorescence microscopy with an Axiophot microscope (Zeiss Optical, Petersburg, VA).

Immunogold Localization of BSA by Transmission EM. To determine ultrastructural localization of monomeric BSA exit pathways in the cerebral microvasculature in experimental meningitis, immunogold labeling of in situ perfused monomeric BSA was performed by both pre- and post-embedding methods.

Pre-embedding Immunogold Diffusion Method. After in situ perfusion and fixation, the brain was cut into 1-mm coronal slices, frozen in liquid N_2, and cryosectioned (10-μm thickness) with a Frigocut (Reichert Scientific Instruments). Sections were incubated with the primary rat anti-BSA antibody (1:50 in PBSO) for 18 h, washed in PBSO for 1 h, and reincubated for 18 h in goat-anti-rat IgG coupled to 5 nm gold. After washing again in PBSO for 1 h, the tissue was subjected to the following steps: (*a*) fixation in 1.5% glutaraldehyde in 0.1 M cacodylate and 5% sucrose for 1 h; (*b*) post-fixation in 1% OsO_4 in acetate veronal buffer; (*c*) treatment in 2% uranyl acetate followed by graded ETOH dehydration, 50% propylene oxide infiltration, and embedding in Epon 812 on a flat mold. After overnight polymerization at 60°C, brain cortical specimens were cut from the molds, remounted on Epon dummy blocks, and replaced in a 60°C oven for 48 h. Thin sections were then cut, stained with uranyl acetate and lead citrate, and examined by TEM.

Post-embedding Immunogold Labeling of Ultrathin Frozen Sections. Washed tissue blocks were processed according to the method of Tokuyasu (9) as modified by Milici et al. (10), which requires tissue infiltration for 2 h with 50% polyvinylpyrrolidine containing 2.3 M sucrose in 0.1 M phosphate buffer (pH 7.4), followed by mounting on metal nails and freezing in liquid N_2. Thin frozen sections were cut on glass knives with an ultramicrotome provided with an FC-4 cryoattachment (Reichert Scientific Instruments). Sections were then picked up on a drop of 1.92 M sucrose containing 0.75% gelatin in 9 mM phosphate buffer, pH 7.4, and placed on nickel grids. Sections on grids were then floated (section side down) on the following solutions: (*a*) PBS containing 0.1% OVA three times for 10 min; (*b*) rat anti-BSA diluted 1:100 in PBS/0.1% OVA, for 1 h; (*c*) PBS/0.1% OVA washes, six times for 10 min; (*d*) goat anti-rat IgG-Au_5, diluted 1:500 in PBS/0.1% OVA; (*c*) repeat washing step as in step *c*; (*f*) fix in 2% glutaraldehyde for 10 min; (*g*) wash with PBS for 10 min, and then with ddH_2O for 2 min; (*h*) post-fix in 2% O_sO_4 for 20 min; (*i*) wash with ddH_2O for 2 min; (*j*) stain with 2% uranyl acetate for 15 min; (*k*) 2.5% polyvinyl alcohol containing 0.0015% lead citrate, twice for 2.5 min. Grids were then air dried after removing excess fluid and examined by TEM.

Morphometry. To determine the percentage of labeled plasmalemmal vesicles, we examined 10 random low magnification (×18,000) micrographs of cross-sectioned pial microvessels (arteriolar, venular, capillary) in control and LPS-inoculated rats perfused with colloidal gold-BSA tracer in situ.

Results

Natural History of Experimental Meningitis

To initially characterize the natural history of the experimental subarachnoid inflammation, experiments were performed documenting the kinetics of CSF inflammation and functional ^{125}I-BSA entry after intracisternal LPS inoculation. As shown in Fig. 1, after intracisternal inoculation of 25 ng of *E. coli* 0111:B4 LPS, a significant CSF leukocyte exudation (mean ± SE WBC = 5.82 ± 2.2 × 10^3) began 3–4 h later, peaked at 6 h (mean ± SE WBC = 14.1 ± 4.4 × 10^3), and was reversible by 24 h. Similarly, there was a significant functional BBB injury (as determined by CSF penetration of systemically administered ^{125}I-BSA) that began 3 h post-inoculation (mean ± SE% CSF ^{125}I-BSA = 1.42 ± 0.6), peaked at 4 h (mean ± SE% CSF ^{125}I-BSA = 2.7 ± 0.8), and was reversible by 24 h (see Fig. 2). To

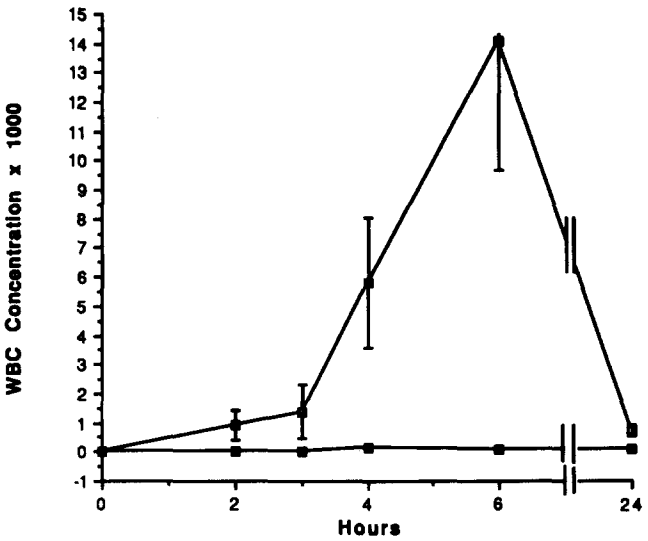

Figure 1. Kinetics of CSF leukocytosis during experimental meningitis. Depicited is CSF leukocyte concentration vs. time (h) after intracisternal inoculation of rats with 25 ng *E. coli* 0111:B4 LPS (*open squares*) or saline (*closed squares*).

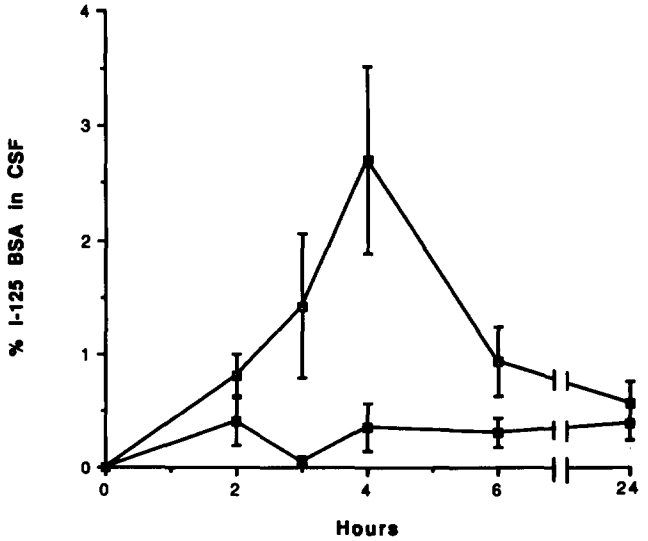

Figure 2. Kinetics of ^{125}I-BSA penetration into CSF during experimental meningitis. Depicited is percent ^{125}I-BSA CSF penetration vs. time (h) after intracisternal inoculation of rats with 25 ng *E. coli* 0111:B4 LPS (*open squares*) or saline (*closed squares*).

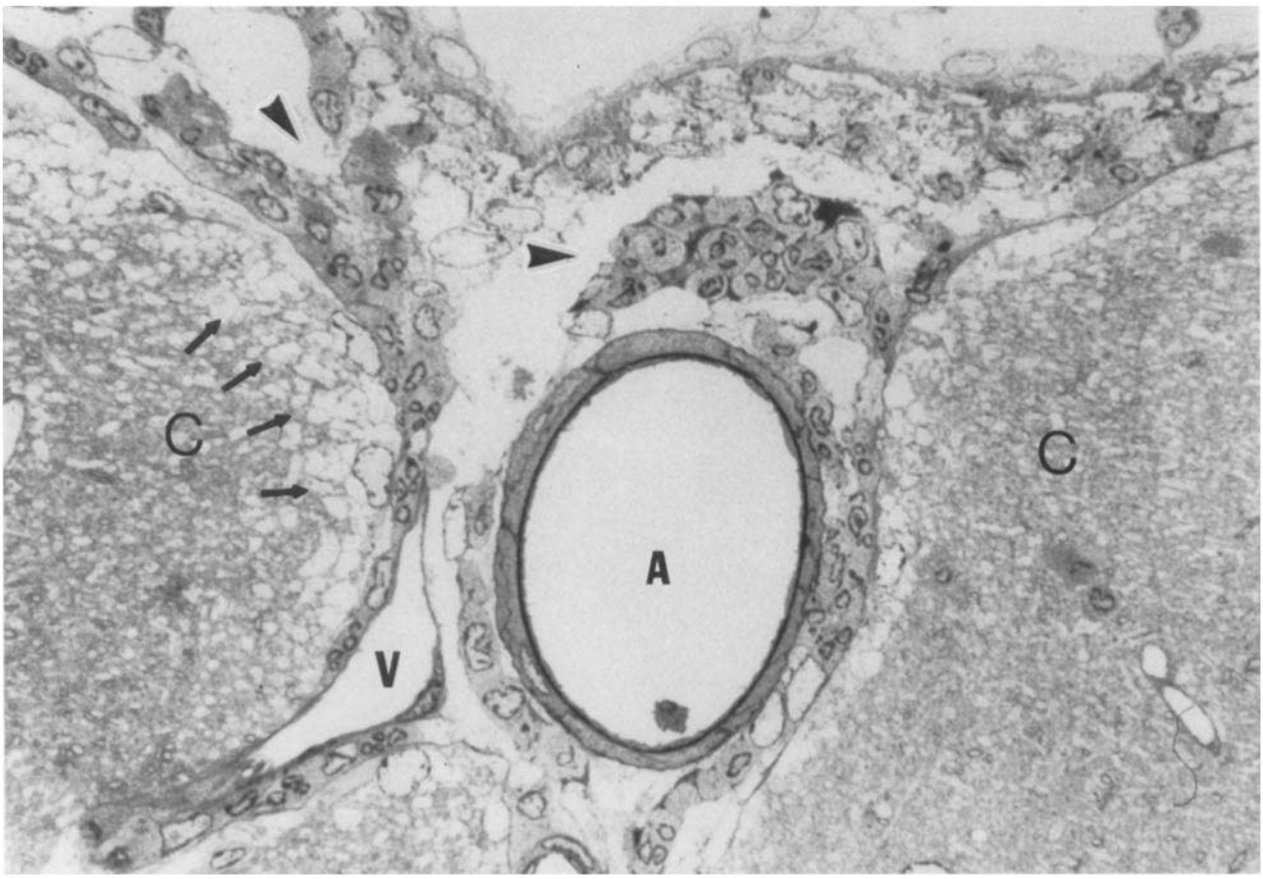

Figure 3. Light micrograph (×63) of superficial brain cortex and meninges. Depicited is pia-arachnoid inflammation (*arrows*) as well as subcortical brain edema after 4 h of experimental meningitis. A, arteriole lumen; C, brain cortex; V, venule.

confirm histologically leptomeningitis, 4 h post-intracisternal LPS inoculation, rats were perfusion fixed in situ, specimens from the superficial brain were collected, processed, embedded, and sectioned (5 μm) on an ultramicrotome, and stained with methylene blue. As seen in Fig. 3, light microscopy (×63) of superficial brain revealed pia-arachnoid inflammation as well as subcortical brain edema documenting gross histologic injury at a time of significant functional disease.

In Situ Tracer Perfusion during Experimental Meningitis

Colloidal Gold BSA Perfusion. To localize ultrastructurally the pathways of BSA exit out of the CNS microvasculature during active meningitis, rats were perfused in situ with colloidal gold coupled to BSA 4 h after intracisternal LPS inoculation, and the superficial brain cortical microvasculature was examined by TEM. As seen in Fig. 4, there was significant uptake of Au-BSA into plasmalemmal vesicles (PV) of the pial microvasculature (of infected rats) compared to uninfected controls. To rule out nonspecific binding facilitated by the glutamic acid stabilizer, additional control experiments were done in which infected rats were perfused in situ with Au-BSA (stabilized with glutamic acid) or Au-glutamic acid alone. As shown in Fig. 5, there was similar uptake of Au-BSA into coated vesicles as well as binding to uncoated pits of the pial microvasculature, but negligible uptake of Au-glutamic acid in a similarly infected rat. To morphometrically quantitate the degree of labeling of PV, 10 random micrographs of pial microvessels were examined from LPS-infected and PBS control rats 4 h post-inoculation. As seen in Table 1, there was significant and similar uptake of Au-BSA into PV of all microvascular segments of infected, but not control pia-arachnoid microvessels. However, no evidence of transcytosis of Au BSA was detected over the intervals examined.

When the possibility for paracellular leak of BSA was investigated, there was striking evidence for Au-BSA traversal through open intercellular junctions to the perivascular space (see Fig. 6). In contrast to the Au-BSA uptake into PV (which occurred in all segments of the pial microvasculature), paracellular Au-BSA exit through open intercellular junctions was topographically restricted to inflamed venules of the pia-arachnoid.

Carbon Black Perfusion. To determine the frequency of such paracellular leaks, large fields were examined at very low magnification in a separate series of experiments in which rats were perfusion fixed in situ with 0.01% carbon black-

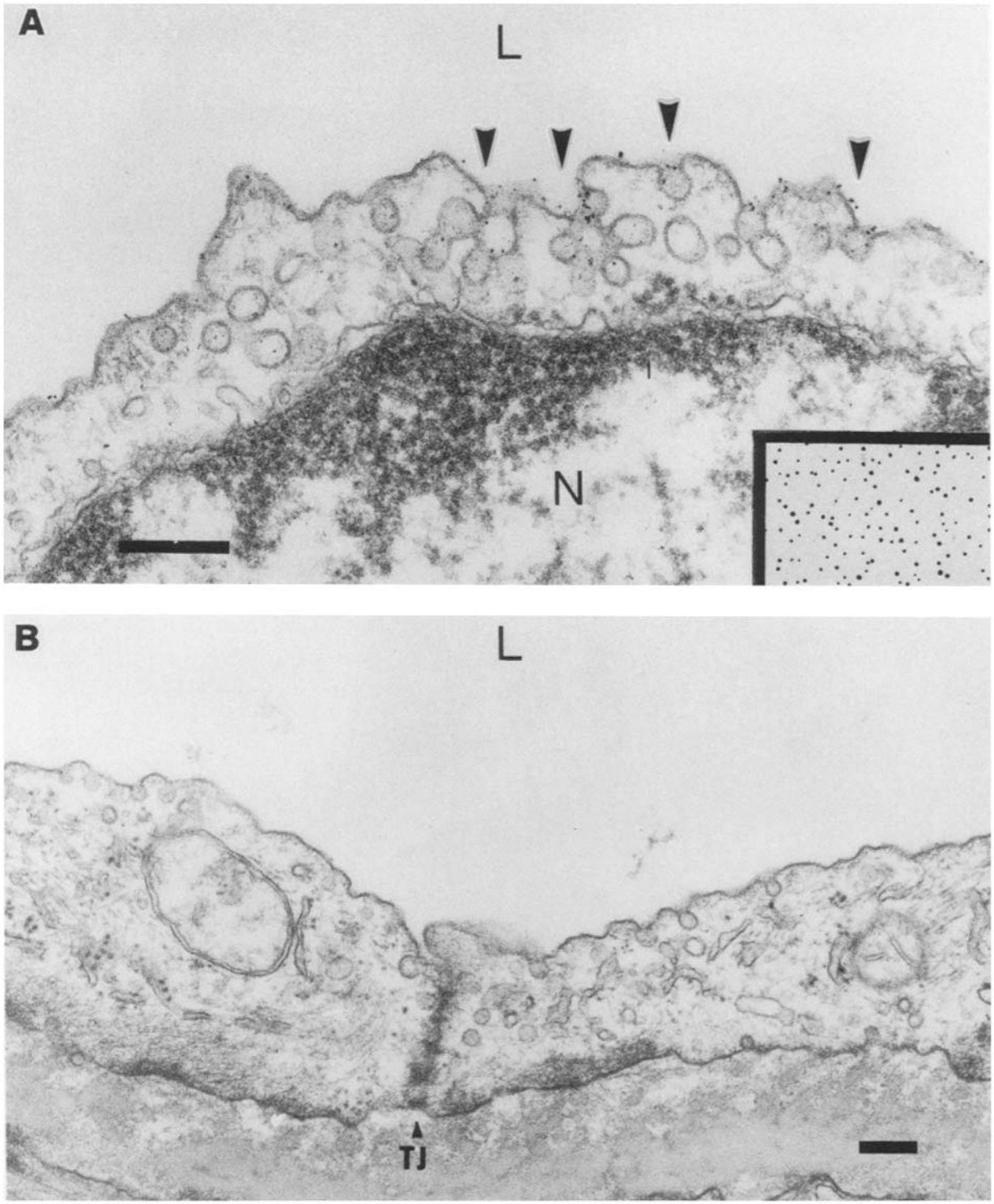

Figure 4. Interaction of in situ perfused colloidal Au-BSA with pial microvasculature during experimental meningitis. Note the uptake (*arrows*) of Au-BSA into PV, of a pial arteriole after 4-h experimental meningitis (*A*) compared with saline controls (*B*). L, vessel lumen; N, nucleus; TJ, intercellular tight junction of pial venule. Inset shows monodispersity of colloidal Au-BSA complexes before perfusion. Bar = 0.2 μM.

3% glutaraldehyde after various durations of experimental meningitis. As shown in Fig. 7, compared to uninflamed controls (Fig. 7 *a*), there was significant evidence for focal leak of carbon black out of large and small pial venules after 4 h of experimental meningitis (Fig. 7, *b* and *c*). This was also significant compared to the negligible leak after 2-h (Fig. 7

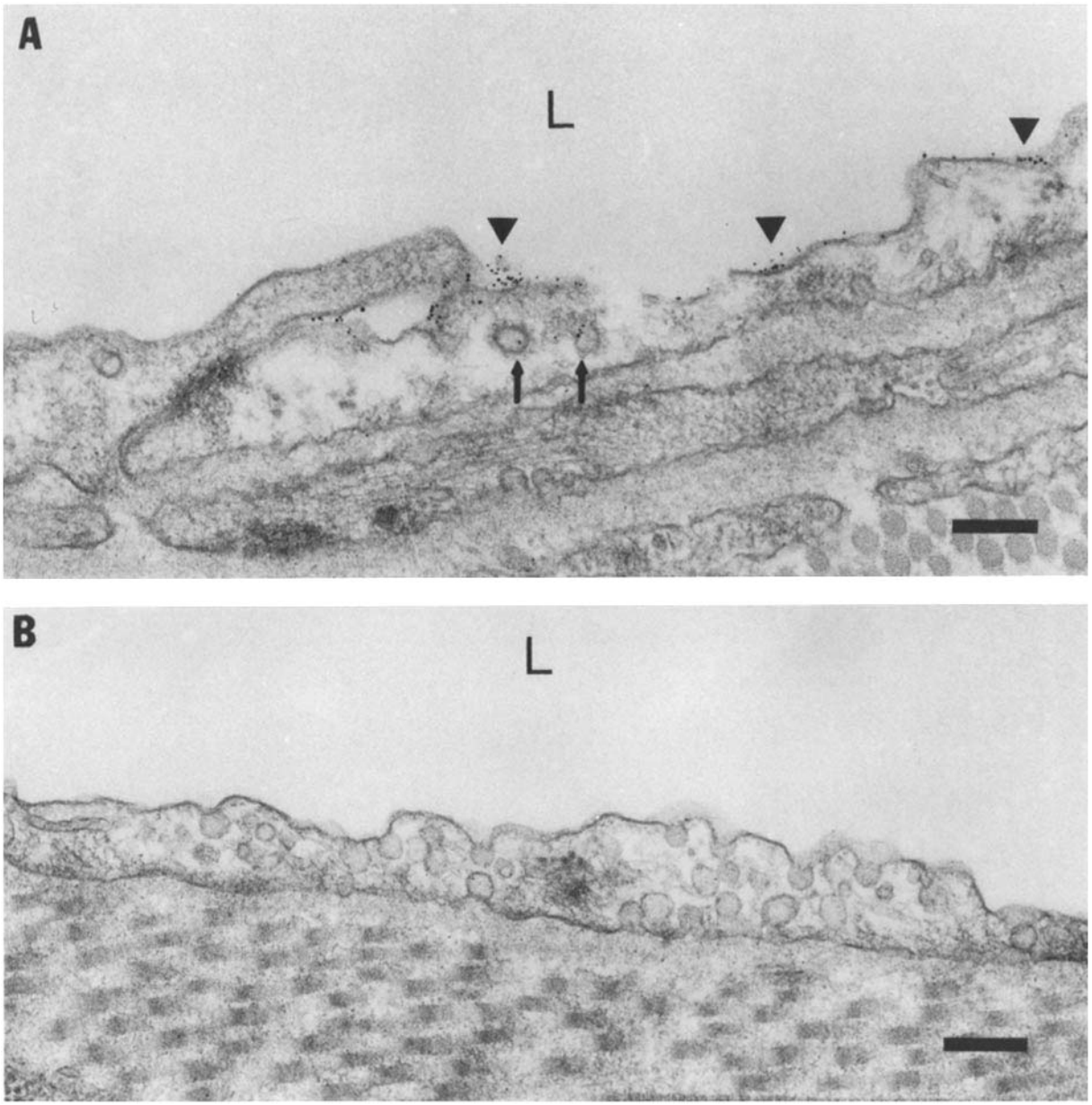

Figure 5. Interaction of in situ perfused colloidal Au-BSA (*A*) vs. colloidal Au glutamic acid (*B*) with pial microvasculature during experimental meningitis. Note the uptake of Au-BSA into PV of a pial venule (*arrows*) as well as uncoated pits (*arrowheads*) after 4 h of experimental meningitis (*A*). However, after similar duration (4 h) of experimental meningitis, there was no binding or uptake of Au glutamic acid (without BSA) anywhere in the pial microvasculature. L, vessel lumen. Bar = 0.2 μM.

d) and 24-h infection durations (Fig. 7 *e*), time points in which functional CSF ^{125}I-BSA traversal was previously documented to be insignificant.

Immunolabeling of Monomeric BSA during Experimental Meningitis

To obtain additional confirmatory evidence for BSA exit pathways, a series of experiments were performed in which in situ perfused monomeric BSA (40 mg/ml) was immunolocalized with an affinity-purified rat anti-BSA antibody at the light and EM level. The anti-BSA antibody was raised in rats to elicit specificity for BSA over endogenous rat serum albumin (RSA). After immunization, serum was harvested and antibody was purified by protein G affinity chromatography with confirmation as a 180-kD band (nonreduced) by SDS-PAGE (data not shown). To determine the sensitivity and specificity of the purified antibody for BSA (vs. RSA) in the face of fixation, a series of ELISAs were performed. As shown in Fig. 8, the primary antibody sensitivity for BSA and specificity (vs. RSA) was achieved in the face of 4% paraformaldehyde even when supplemented with 0.5%

Table 1. *Quantitation of In Situ Perfused Au-BSA Labeling of PV in Pial Microvasculature*

Rats		No. of PV	No. of labeled PV
			%
LPS inoculated	Capillary	45	16 (36)
	Venule	116	38 (33)
	Arteriole	81	23 (28)
Control	Capillary	11	0 (0)
	Venule	55	1 (2)
	Arteriole	73	0 (0)

glutaraldehyde. Hence, this fixation combination was then used for immunolocalization in situ.

Immunofluorescent Localization. As the initial step in immunolocalization of BSA in situ during experimental meningitis, rats were perfused with monomeric BSA 4 h after LPS intracisternal inoculation. After in situ fixation, brain and heart were frozen, cryosectioned, and BSA was localized by immunofluorescence microscopy. The heart served as a positive control and the procedure allowed the examination of large fields including many vessels. As shown in Fig. 9, the rat anti-BSA antibody specifically localized BSA in the heart in all cross-sectioned microvessels (Fig. 9, *a* and *b*) as well as the pia-arachnoid microvasculature after LPS-induced inflammation (Fig. 9, *c* and *d*); uninflamed pia-arachnoid from saline-inoculated rats showed no detectable fluorescence. This suggested that immunogold localization of BSA by transmission EM was feasible.

Immunogold Localization. To immunolocalize BSA by TEM two complementary immunogold techniques were utilized.

Pre-embedding Immunogold Labeling. Results of the pre-embedding immunogold diffusion technique are depicted in Fig. 10. As shown in Fig. 10, *a* and *b*, after 4 h of experimental meningitis, there was immunodetection of enhanced BSA binding to the luminal membrane of a pial microvessel as well as immunolocalization within the perivascular space after a 10-min monomeric BSA perfusion. Although a venule is depicted in the micrograph, similar enhanced luminal membrane BSA binding was observed in arterioles and capillaries as well. When intercellular junctions were examined, there was immunogold detection of BSA exit through open intercellular junctions, corroborating that observed in Au-BSA experiments (Fig. 10 *c*). When the superficial brain microvasculature was examined, there was a similar enhanced luminal membrane binding of BSA after a 10-min perfusion in rats with experimental meningitis compared to controls (Fig. 10, *d* and *e*). However, as opposed to the pial microvasculature, there was no evidence of BSA in the perivascular space or exit via intercellular junctions. To assess if a shorter BSA perfusion time would yield similar results, rats were perfused with the same concentration of monomeric BSA (40 mg/ml) for 1 min after a 4-h experimental meningitis. As documented in Fig. 10 *f*, there is less immunogold detection of BSA binding to the luminal membrane as well as less (but present) immunogold label in the perivascular space of a pial microvessel.

Post-embedding Immunogold Labeling. Since the pre-embedding immunogold diffusion method is incapable of detecting intracellular albumin tracer, such as found in other endothelia in transcellular transport via plasmalemmal vesicles, direct immunogold labeling of ultrathin frozen sections were done. As shown in Fig. 11, there was immunodetectable BSA within some PV of a pial capillary (as well as in the perivascular space) after 4 h of experimental meningitis. However, similar to the Au-BSA experiments, only a minority of the PV were labeled.

Discussion

In this inquiry, we sought to identify the microvascular subcellular pathway(s) of albumin exit across the blood brain barrier during experimental meningitis. Using a rat model of CSF inflammation, we investigated, at the ultrastructural level, albumin transport by vascular perfusion of colloidal gold–albumin complexes as well as monomeric albumin (BSA) localized in situ by an immunogold procedure. The salient results suggest that during meningitis, the primary site of albumin exit is at the pia-arachnoid microvasculature, predominates in the venular segments, and occurs primarily via a paracellular pathway through open intercellular junctions.

As a disease, bacterial meningitis accounts for worldwide morbidity and mortality despite the fact that available antibiotics can achieve CSF bactericidal activity and are capable of rapid bacteriologic cure. Mounting evidence in animal models and humans suggests that induction of inflammatory cytokines within the CSF, before and during bacteriolysis, initiate and perpetuate CSF neutrophil and albumin exudation across the BBB (11–13). The resultant altered CSF milieu facilitates both vasogenic and cytotoxic brain edema and is associated with disturbed cerebrovascular autoregulation (14); a pathophysiology capable of precipitating neuronal injury, seizures, and death.

In the context of previous investigation correlating ultrastructural alterations of isolated cerebral microvessels with functional BBB injury (8), we now report detailed ultrastructural observations on albumin exit pathways in situ at the subcellular level in the microvascular endothelium of pia-arachnoid and cerebral cortex. As the initial step, the kinetics of leukocyte and ^{125}I-BSA exudation into CSF were characterized in an experimental rat model. As shown in Figs. 1–3, intracisternal inoculation of *E. coli* 0111:B4-purified LPS induced a reversible CSF inflammation and BBB injury that peaked at 4–6 h, with histologic confirmation of gross leptomeningitis by light microscopy.

After confirming this time point of peak functional injury, initial investigations into BSA exit pathways were performed by in situ tracer perfusion of colloidal gold Au-BSA complexes. This particular tracer has been recently demonstrated to be useful in ultrastructural definition of albumin exit pathways in normal systemic and CNS microvasculature. Specifically, using mouse and rat in situ perfusion models,

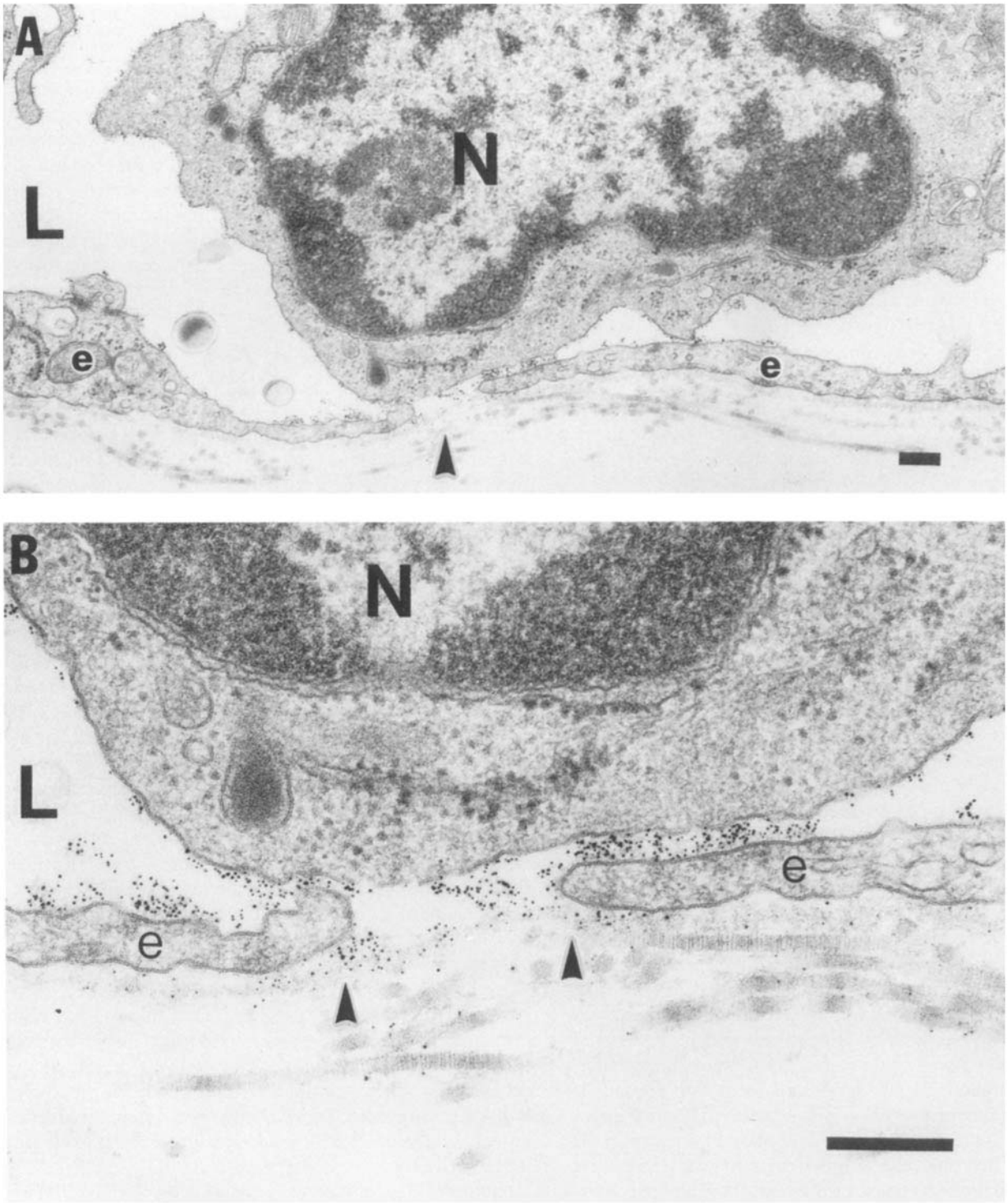

Figure 6. Traversal of in situ perfused Au-BSA out an open intercellular junction (*arrowheads*) of a pial venule after 4 h of experimental meningitis at low (*A*) and high (*B*) magnification. L, vessel lumen; e, venular endothelium; N, nucleus of marginated leukocyte. Bar = 0.2 μM.

there appears to be specific albumin binding to endothelial PV as well as transcytosis in systemic (6), but not CNS microvasculature (15). Therefore, using a similar protocol, we could observe whether during inflammation, the CNS microvasculature employs albumin transcytosis or uses a paracellular route. As shown in Fig. 4, after 4 h of experimental meningitis, there was evidence for significant uptake of Au-BSA by PV in the pial microvasculature compared to uninflamed controls. Although there was some limited Au-BSA binding to the plasmalemma proper, there was preferential

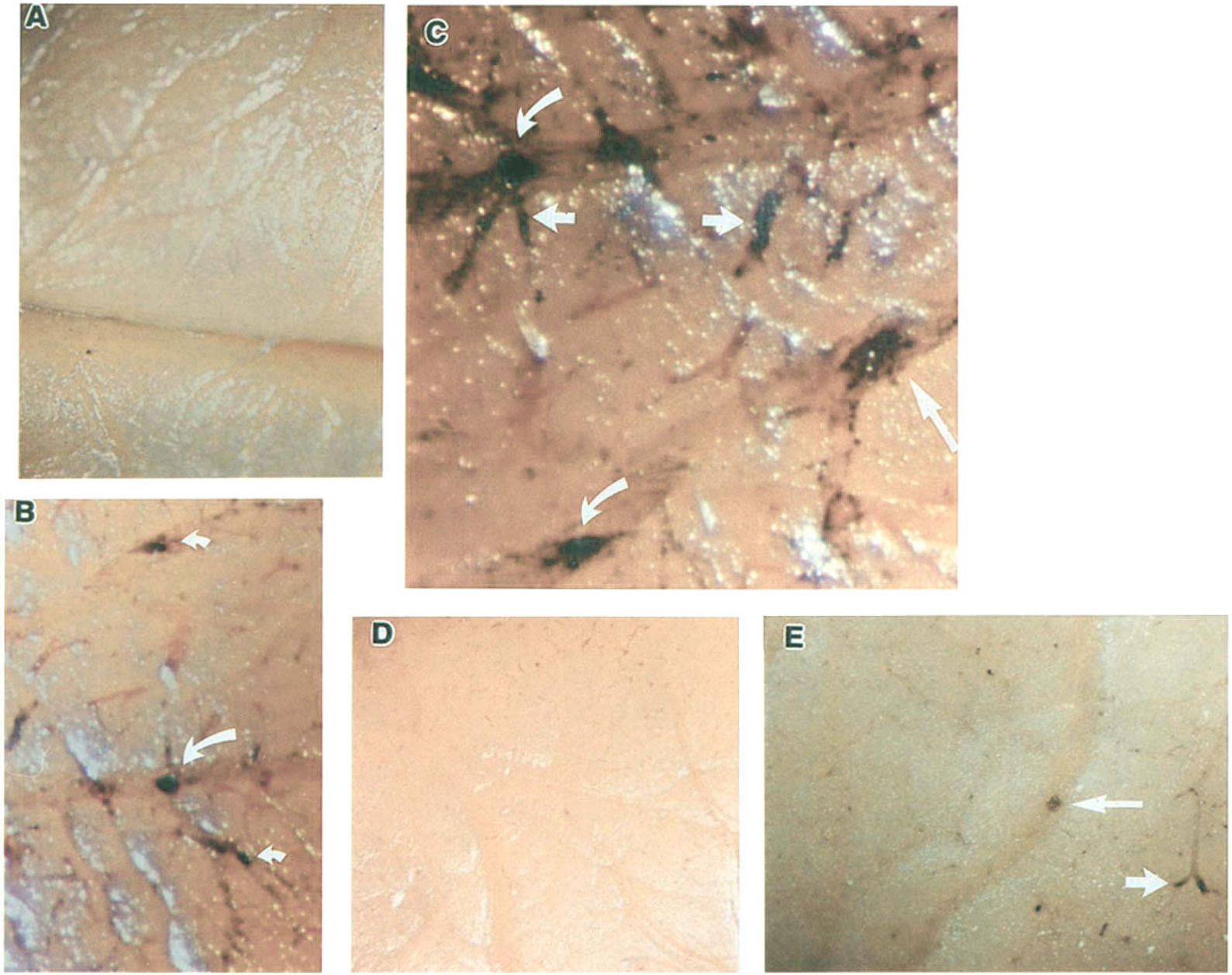

Figure 7. Results of in situ perfusion of carbon black during experimental meningitis. (*A*) Pial surface of control rat 4 h post-inoculation with PBS; (*B*) and (*C*) pial surface of rat 4 h post-inoculation with LPS. Note focal areas of carbon black leak from large and small venules (*arrows*). (*D*) Negligible carbon black leak 2 h post-LPS inoculation; (*E*) minimal, but present, carbon black leak from pial venules 24 h post-LPS inoculation. Bar = 0.2 μM.

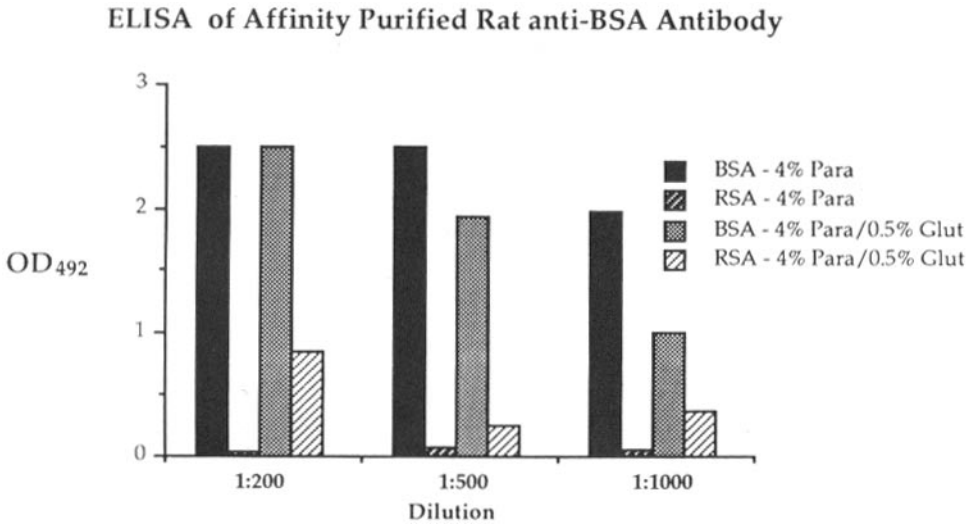

Figure 8. ELISA of affinity-purified rat anti-BSA antibody at various dilutions. Note the sensitivity and specificity for BSA (vs. RSA) under conditions of 4% paraformaldehyde/0.5% glutaraldehyde fixation.

binding to PV and uncoated pits. Poly-L-glutamic acid was utilized as a colloidal gold complex stabilizer given problems faced in pilot experiments in which other stabilizers (e.g., polyethylene glycol) caused nonspecific binding to microvascular luminal membranes. We reasoned that the anionic charge of poly-L-glutamic acid at neutral pH would reduce the possibility of nonspecific electrostatic binding of the colloidal-Au complexes to the endothelium. Indeed, this hypothesis was supported by the control experiments documenting negligible binding of Au-glutamic acid alone to inflamed pial microvasculature (Fig. 5). Nonetheless, even during meningitis only a minority of the PV were labeled (Table 1), and there was no evidence of selective vesicle membrane binding or transcytosis to the abluminal surface as described by Ghitescu et al. (6) in uninflamed systemic microvasculature, within the time intervals tested. The increased labeling of endothelial plasmalemmal vesicles in inflamed specimens without evidence of detectable transcytosis implies that plasmalemmal vesicles may not perform a common function (i.e., macromolecular transcytosis) in all endothelia.

Upon further ultrastructural examination, the only vessels where Au-BSA was visualized in the perivascular space were pial venules in which there was paracellular leak of Au-BSA through open intercellular junctions (Figure 6). To compensate for sampling limitations inherent in electron microscopy, this finding was corroborated on large samples of tissues perfused with an appropriate tracer, 0.01% carbon black (in 3% glutaraldehyde), and examined at low optical magnifications (Fig. 7). Perfused carbon black leaks through open intercellular junctions but is limited by the vessel's basement membrane, thereby labeling such injured vascular segments. As demonstrated, there was evidence for focal leaks of carbon black primarily out of small and large pial venules, and these leaks showed similar reversible kinetics to the functional ^{125}I-BSA CSF efflux previously demonstrated (Fig. 2). This focal venular pattern of tracer leaks is very reminiscent of that originally described by Majno and Palade (16) in cremasteric microvasculature as a response to the inflammatory mediators histamine and serotonin. However, the tracer leaks in the inflamed pial microvasculature were more scattered and not exclusively associated with post-capillary venules.

Nonetheless, in our experiments, limitations remain in the interpretation of endothelial exit pathways of Au-BSA complexes since it is a polymeric tracer with a documented slower rate of endothelial transcytosis than monomeric BSA (10). Therefore, immunolabeling studies of perfused monomeric BSA were necessary as a corroborative investigation. Specifically, rat anti-BSA antibody was purified, tested for specificity under various fixation conditions by ELISA (Fig. 8), and utilized to immunolocalize monomeric BSA in situ during experimental meningitis. After initial experiments documented the ability of this antibody to specifically localize BSA by immunofluorescence in situ (Fig. 9), we tested two complementary immunogold detection methods to localize perfused monomeric BSA during meningitis by TEM. The pre-embedding immunogold diffusion labeling protocol (Fig. 10) allowed for immunogold labeling of BSA with excellent ultrastructural preservation but could not detect antigen (BSA) at intracellular sites (i.e., PV) involved in transcytosis. The post-embedding, direct immunogold labeling of ultrathin frozen sections provided the opportunity to observe labeling of vesicles (10), but at the expense of poorer ultrastructural preservation of the inflamed microvasculature.

Results of the pre-embedding immunogold diffusion method (Fig. 10) provided two important ultrastructural observations. First, during meningitis, there appears to be augmented monomeric BSA binding to the luminal endothelial membrane of microvasculature (arterioles, capillaries, and venules) in the pia-arachnoid as well as superficial brain cortex. Second, monomeric BSA can be immunolocalized to exit pial venules via open intercellular junctions similar to that observed with perfused Au-BSA complexes. Noteworthy is that the paracellular leak was through an intercellular junction in which there was no concomitant leukocyte adherence, suggesting that the two phenomena are not interrelated. The post-embedding labeling of ultrathin frozen sections corrobo-

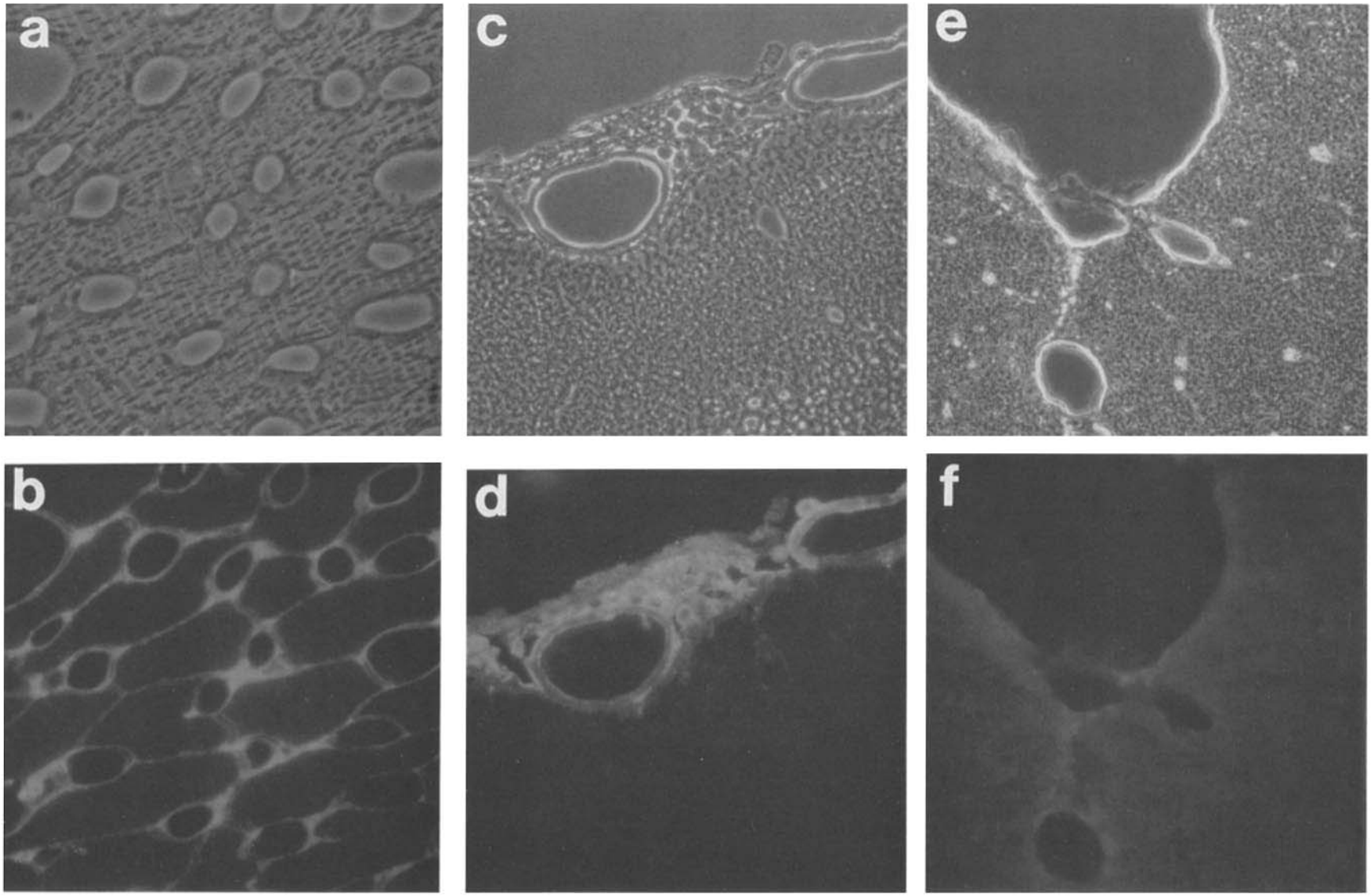

Figure 9. Immunofluorescent localization of BSA in situ. (*a* and *b*) Phase and fluorescence microscopy of myocardial microvasculature in cross-section after a 10-min BSA (40 mg/ml) perfusion; (*c* and *d*) phase and fluorescence of pial surface in cross-section after a 10-min BSA perfusion 4 h post-LPS inoculation; (*e* and *f*) phase and fluorescence of pial surface in cross-section after a 10-min BSA perfusion in a control animal 4 h post-saline inoculation.

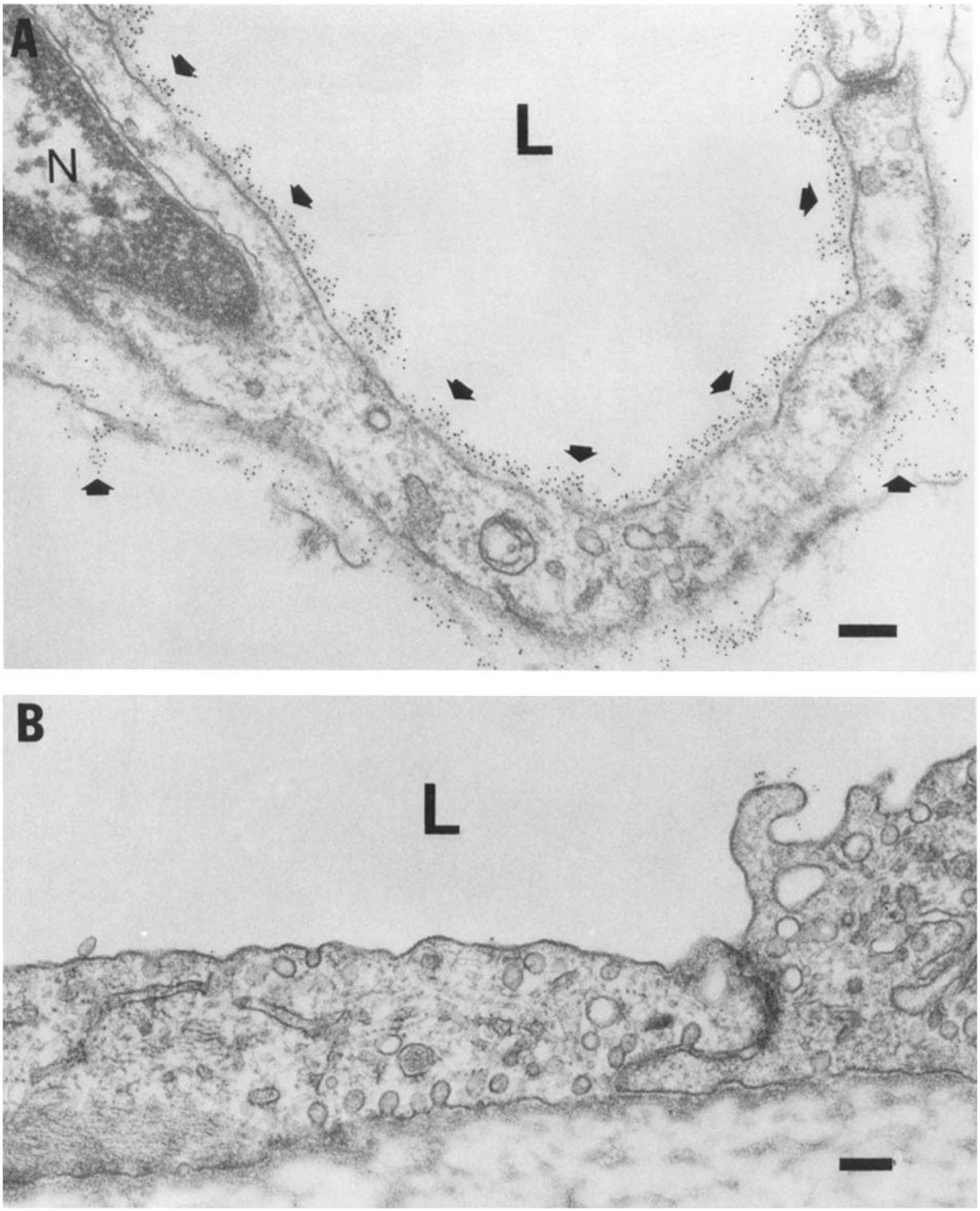

Figure 10. Pre-embedding immunogold diffusion labeling of BSA by TEM. (*A*) Enhanced BSA binding to the luminal membrane of a pial venule after 10-min BSA perfusion, 4 h post-LPS inoculation. Note the presence of immunodetectable BSA in the perivascular space (*arrows*) as well. (*B*) Negligible BSA binding to the pial microvasculature in a saline control rat. (*C*) Immunogold detection of enhanced luminal membrane binding of BSA, as well as exit through an open intercellular junction in a pial venule after 4 h of experimental meningitis. (*D*) Similiar enhanced BSA binding to the luminal membrane of a capillary in the superficial brain cortex after 4 h of experimental meningitis. (*E*) Negligible BSA binding to superficial brain microvessels in saline-inoculated control rats. (*F*) Less extensive immunogold detection of BSA binding to the luminal membrane, as well as within the perivascular space (*arrowheads*) with a 1-min BSA perfusion, after 4 h of experimental meningitis. L, lumen; e, endothelial cell; N, nucleus of endothelial cell. Bar = 0.2 μM.

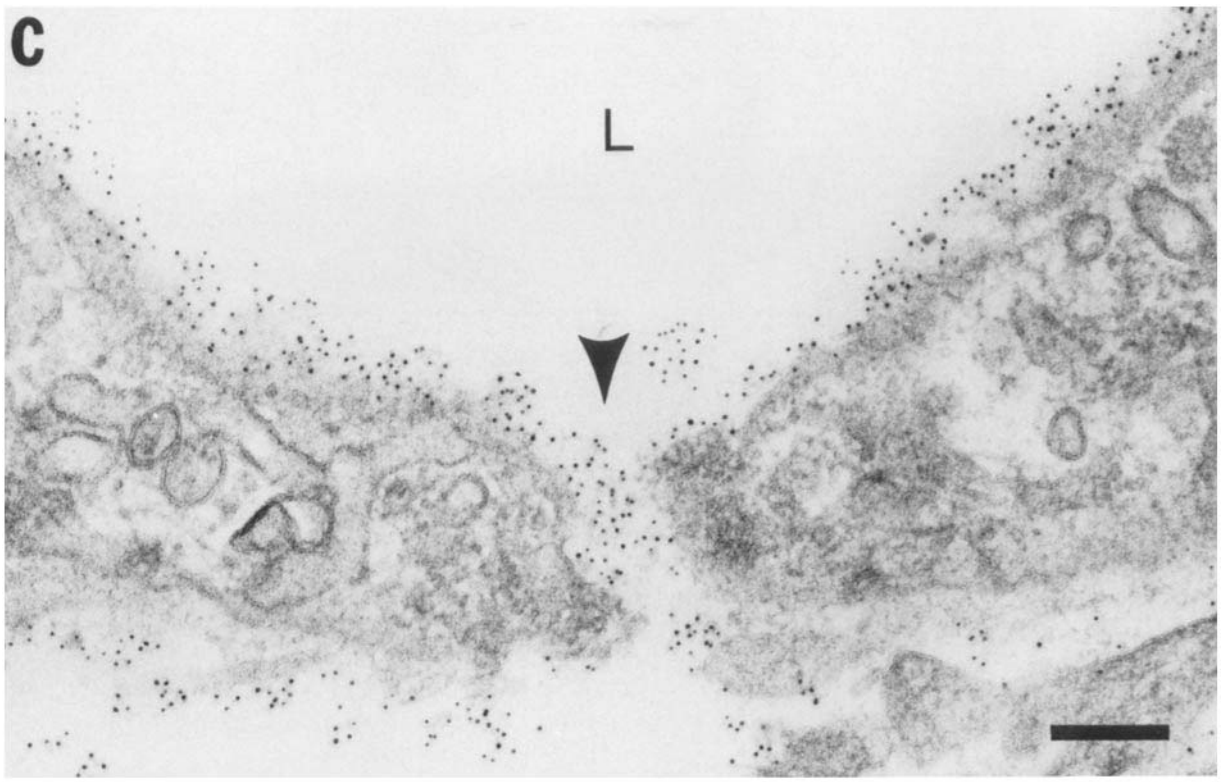
C
L

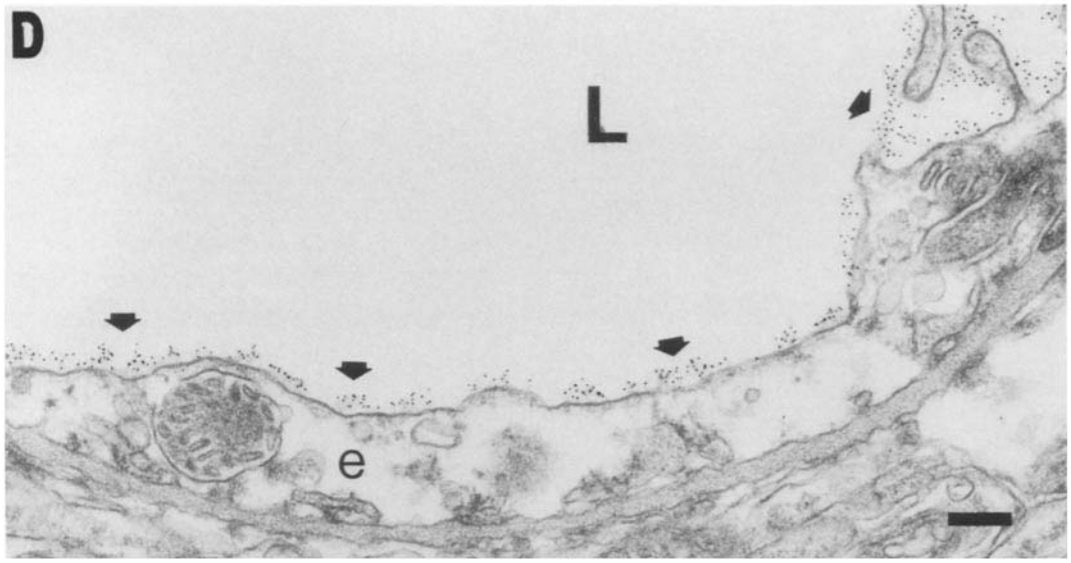
D
L
e

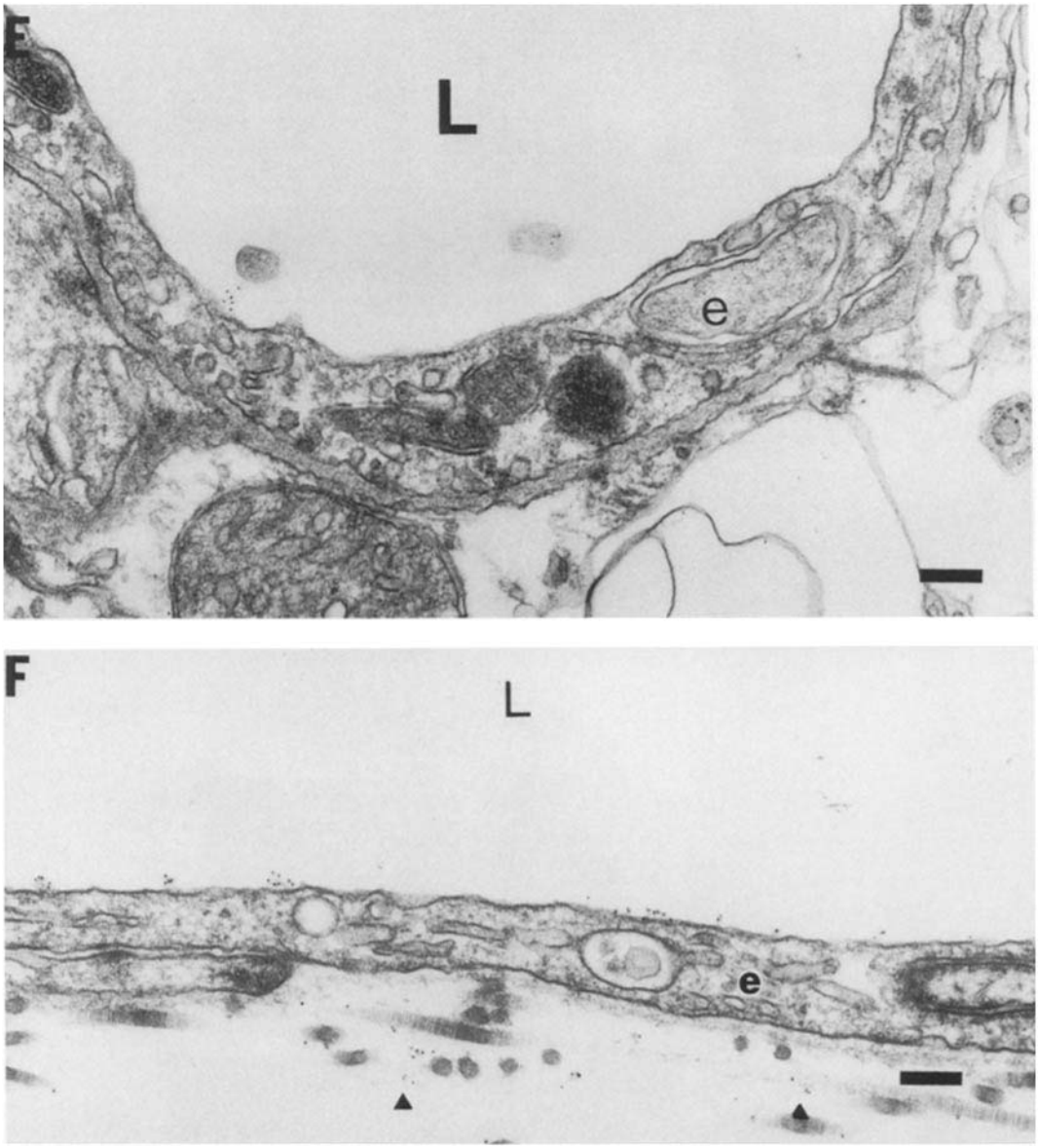

rated this and revealed that although there was immunodetectable BSA within some PV of pial capillaries during experimental meningitis, only a minority were labeled (Fig. 11), as was noted in the Au-BSA perfusion studies.

The detection of enhanced monomeric BSA binding to the luminal membrane (not seen with polymeric Au-BSA complexes) may relate to the higher concentration of BSA perfused (40 mg/ml of monomeric BSA vs. 80 μg/ml of BSA in Au-BSA perfusate) or more efficient expression of ligand binding sites on monomeric albumin. Nonetheless, the observation is intriguing and may suggest binding of albumin to specific albumin-binding proteins (17, 18), or other inducible adhesive glycoproteins expressed on endothelium in response to inflammatory peptides (e.g., ELAM-1, ICAM-1, GMP-140) during meningitis (19–21).

The finding of albumin exit via open intercellular junctions of pial venules by both immunolabeling BSA and in situ perfusion of Au-BSA complexes strongly supports this paracellular route as the major exit pathway during meningitis and confirms a previously unproven assumption based on in vitro and in situ observations in systemic microvasculature. Specifically, the systemic post-capillary venule has been shown to exhibit loosely organized intercellular junctions (compared to capillaries and arterioles) that open during vasoactive amine exposure (i.e., histamine) allowing for paracellular protein leak (16, 22). The in situ localization of histamine receptors in high concentration in the plamalemma overlying the perijunctional area rich in actin and myosin further support this concept (23). Whether histamine is a primary mediator within the central nervous system, and whether its regulation of endothelial contractility and paracellular leak is via cytosolic calcium (as shown in vitro [24]) remain conjectural but testable hypotheses. Likewise, this paracellular route of albumin exit could result from an effect of locally produced

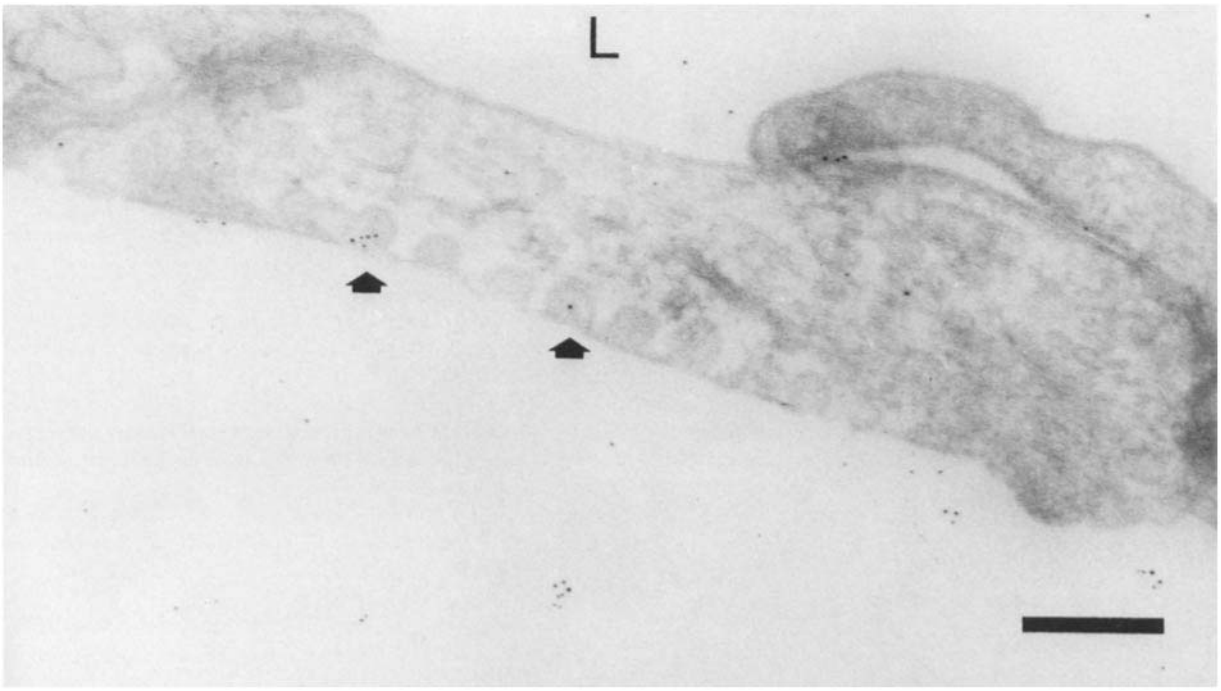

Figure 11. Direct immunogold labeling of BSA on ultrathin frozen section (post-embedding). Note the immunogold detection of BSA within some plasmalemmal vesicles (*arrows*) as well as within the perivascular space. L, lumen. Bar = 0.2 μM.

inflammatory cytokines (IL-1, TNF) directly on the endothelium itself. This is supported by observations in which both TNF and IL-1 have been shown to induce both a time- and dose-dependent increase in endothelial cell monolayer permeability to albumin in vitro (25). Further studies have correlated endothelial monolayer permeability alterations to a direct TNF induction of cytoskeletal changes and intercellular gap formations, a pathologic response that appears to be regulated by a pertussis toxin–sensitive G protein (26).

Nonetheless, the observations made in this experimental model provide consistent and precise localization of BBB injury in meningitis to meningeal venules, confirm exit of albumin via open intercellular junctions in situ, and provide a fundamental premise upon which to design adjunctive therapeutic agents for human disease.

Vincent J. Quagliarello is supported by a Physician-Scientist Award (5-K11-HL02062-03) from the National Institutes of Health.

Address correspondence to Vincent Quagliarello, LCI 800, Division of Infectious Diseases, Yale University School of Medicine, 333 Cedar Street, New Haven, CT 06510. George E. Palade's current address is the University of California, San Diego, CA.

Received for publication 15 February 1991 and in revised form 29 May 1991.

References

1. Swartz, M. 1984. Bacterial meningitis. More involved than just the meninges. *N. Engl. J. Med.* 311:912.
2. Reese, T., and M. Karnovsky. 1967. Fine structural localization of a blood-brain barrier to exogenous peroxidase. *J. Cell Biol.* 34:207.
3. Brightman, M., and T.S. Reese. 1969. Junctions between intimately opposed cell membranes in the vertebrate brain. *J. Cell Biol.* 40:648.
4. Bradbury, M.W. 1984. The structure and function of the blood-brain barrier. *Fed. Proc.* 43:186.
5. Crone, C., and S.P. Oleson. 1982. Electrical resistance of brain microvascular endothelium. *Brain Res.* 241:49.
6. Ghitescu, L., A. Fixman, M. Simionescu, and N. Simionescu. 1986. Specific binding sites for albumin restricted to plas-

malemmal vesicles of continuous capillary endothelium: receptor mediated transcytosis. *J. Cell Biol.* 102:1304.
7. Muhlpfordt, H. 1982. The preparation of colloidal gold particles using tannic acid as an additional reducing agent. *Experientia.* 38:1127.
8. Quagliarello, V.J., W.J. Long, and W.M. Scheld. 1986. Morphologic alterations of the blood-brain barrier with experimental meningitis in the rat. Temporal sequence and role of encapsulation. *J. Clin. Invest.* 77:1084.
9. Tokuyasu, K.T. 1986. Application of cryoultramicrotomy to immunocytochemistry. *J. Microsc. (Oxf.).* 143:139.
10. Millici, A.J., N.E. Watrous, H. Stukenbrok, and G.E. Palade. 1987. Transcytosis of albumin in capillary endothelium. *J. Cell Biol.* 105:2603.
11. Saukkonen, K., S. Saude, C. Cioffe, S. Wolpe, B. Sherry, A. Cerami, and E. Tuomanen. 1990. The role of cytokines in the generation of inflammation and tissue damage in experimental Gram-positive meningitis. *J. Exp. Med.* 171:439.
12. Ramilo, O., X. Saez-Llorens, J. Mertsola, H. Jafari, K. Olsen, E. Hansen, M. Yoshinaga, S. Ohkawara, H. Naariuchi, and G. McCracken. 1990. Tumor necrosis factor α/cachectin and interleukin 1β initiate meningeal inflammation. *J. Exp. Med.* 172:497.
13. Quagliarello, V.J., B. Wispelwey, W. Long, and W.M. Scheld. 1991. Recombinant human interleukin-1 induces meningitis and blood brain barrier injury in the rat: characterization and comparison with tumor necrosis factor. *J. Clin. Invest.* 87:1360.
14. Tureen, J.H., R. Dworin, S. Kennedy, M. Sachdeva, and M.A. Sande. 1990. Loss of cerebrovascular autoregulation in experimental meningitis in rabbits. *J. Clin. Invest.* 85:577.
15. Simionescu, M., N. Ghinea, A. Fixman, M. Lasser, L. Kukes, N. Simionescu, and G.E. Palade. 1988. The cerebral microvasculature of the rat structure and luminal surface properties during early development. *J. Submicrosc. Cytol. Pathol.* 70:243.
16. Majno, G., and G.E. Palade. 1961. Studies on inflammation: the effect of histamine and serotonin on vascular permeability. An electron microscopic study. *J. Biophys. Biochem. Cytol.* 11:571.
17. Schnitzer, J., W. Carley, and G.E. Palade. 1988. Albumin interacts specifically with a 60-KDa microvascular endothelial glycoprotein. *Proc. Natl. Acad. Sci. USA.* 85:6773.
18. Ghinea, N., A. Fixman, D. Alexandru, D. Popov, M. Hasu, L. Ghitescu, M. Eskenasy, M. Simionescu, and N. Simionescu. 1988. Identification of albumin binding proteins in capillary endothelial cells. *J. Cell Biol.* 107:231.
19. Bevilacqua, M., S. Stengelin, M. Gimbrone, and B. Seed. 1989. Endothelial leukocyte adhesion molecule 1: an inducible receptor for neutrophils related to complement regulatory proteins and lectins. *Science (Wash. DC).* 243:1160.
20. Marlin, S., and T. Springer. 1987. Purified intercellular adhesion molecule-1 (ICAM-1) is a ligand for lymphocyte associated antigen-1 (LFA-1). *Cell.* 51:813.
21. Geng, J.-G., M. Bevilacqua, K. Moore, T. McIntyre, S. Prescott, J. Kim, G. Bliss, G. Zimmerman, and R. McEver. 1990. Rapid neutrophil adhesion to activated endothelium mediated by GMP-140. *Nature (Lond.).* 343:757.
22. Simionescu, M., N. Simionescu, and G.E. Palade. 1975. Segmental differentiations of cell junctions in the vascular endothelium. The microvasculature. *J. Cell Biol.* 67:863.
23. Heltianu, C., M. Simionescu, and N. Simionescu. 1982. Histamine receptors of the microvascular endothelium revealed in situ with a histamine - ferritin conjugate: characteristic high affinity binding sites in venules. *J. Cell. Biol.* 93:357.
24. Rotrosen, D., and J. Gallin. 1986. Histamine type 1 receptor occupancy increases endothelial cytosolic calcium, reduces F-actin and promotes albumin diffusion across cultured endothelial monolayers. *J. Cell Biol.* 103:2379.
25. Royall, J., R. Berkow, J. Beckman, M.K. Cunningham, S. Matalon, and B. Freeman. 1989. Tumor necrosis factor and interleukin-1 increase vascular endothelial permeability. *Am. J. Physiol.* 257:L399.
26. Brett, J., H. Gerlach, P. Nawrith, S. Steinberg, G. Godman, and D. Stern. 1989. Tumor necrosis factor/cachectin increases permeability of endothelial cell monolayers by a mechanism involving regulatory G proteins. *J. Exp. Med.* 169:1977.